Evolution of the nuclear structure approaching ^{78}Ni: β decay of $^{74-78}$Cu

J. Van Roosbroeck, H. De Witte, M. Gorska, M. Huyse, K. Kruglov, D. Pauwels, J.-Ch. Thomas, K. Van de Vel,* and P. Van Duppen†
K. U. Leuven, Instituut voor Kern- en Stralingsfysica, University of Leuven, Celestijnenlaan 200D, B-3001 Leuven, Belgium

S. Franchoo, J. Cederkall, V. N. Fedoseyev, H. Fynbo, U. Georg, O. Jonsson, and U. Köster
ISOLDE, CERN, CH-1211 Genève 23, Switzerland

L. Weissman and W. F. Mueller
National Superconducting Cyclotron Laboratory, Michigan State University, 164 S. Shaw Lane, Michigan 48824-1312, USA

V. I. Mishin
Institute of Spectroscopy, Russian Academy of Sciences, 142092 Troitsk, Russia

D. Fedorov
St. Petersburg Nuclear Physics Institute, 188350 Gatchina, Russia

A. De Maesschalck, N. A. Smirnova, and K. Heyde
Vakgroep Subatomaire en Stralingsfysica, Universiteit Gent, Proeftuinstraat 86, B-9000 Gent, Belgium
(Received 19 October 2004; published 19 May 2005)

A β-decay study of the even mass ^{74,76,78}Cu isotopes toward levels in ^{74,76,78}Zn was performed at the ISOLDE mass separator. The copper isotopes were produced in proton- or neutron-induced fission reactions on ^{238}U, laser ionized, mass separated, and sent to a β-γ detection system. Half-lives, decay schemes, and possible spin configurations were obtained for the copper isotopes. The results are compared with calculations using schematic forces as well as large-scale shell-model calculations with realistic forces.

DOI: 10.1103/PhysRevC.71.054307 PACS number(s): 21.10.−k, 23.40.−s, 25.85.Ec, 27.50.+e

I. INTRODUCTION

The properties of nuclei around the closed proton shell at $Z = 28$ and between the subshell closure at $N = 40$ and the shell closure at $N = 50$ are of particular interest as testing ground for different theoretical approaches. Large-scale shell-model calculations have been performed recently, and comparison with the experimental data available indicate a rather weak subshell closure at $N = 40$ [1–3]. As mentioned in [4], two-neutron separation energies and their differences also indicate a weak shell gap. When going toward more neutron-rich nuclei, the residual interaction, especially the monopole part, plays a determining role in the properties of the quasiparticle states and the interactions among them [5]. Also, specific π-ν correlations that induce deformation when moving away from the $Z = 28$ closed proton shell, as exemplified in $B(E2)$ measurements [6] and the observation of deformed states in ^{66}Fe [7], play a significant role in this region of the nuclear chart, and it is unclear what the role of these correlations will be when approaching the closed $N = 50$ neutron shell. It is therefore important to experimentally explore the specific residual interactions at play between the pf and the *sdg* shells in extremely neutron-rich nuclei. This information also has implications for stellar core collapse models as the electron capture rates depend strongly on these residual interactions [8].

In recent papers, the structure of ^{70}Cu was studied through β-decay studies of ^{70}Ni and ^{70}Cu, laser spectroscopy measurements, and accurate mass measurements [1,2,9]. Researchers discussed the results in terms of large-scale shell-model calculations and addressed the specific question of the importance of the $N = 40$ subshell closure. In this paper, we report on β-decay studies of neutron-rich even-mass copper isotopes ranging from ^{74}Cu to ^{78}Cu; a separate study of the neighbor of the doubly magic closed-shell nucleus $^{78}_{28}$Ni$_{50}$, while a separate paper will report on a β-decay study of the ^{72}Ni-^{72}Cu-^{72}Zn chain [10]. In this way, a systematic study of the evolution of the nuclear structure of the even-even Zn isotopes when approaching the $N = 50$ closed shell is performed and information on the structure of the odd-odd Cu nuclei is obtained as well. The data are compared with calculations using both schematic forces (zero-range δ interaction with spin exchange and quadrupole-quadrupole forces) and small model spaces as well as with large-scale shell-model calculations using realistic effective interactions as given by G-matrix calculations [11] with a modified monopole part [12]. Some of the results on the decay of ^{78}Cu have been published in a conference proceedings [13].

The results obtained from a β-decay study of ^{74,76,78}Cu performed at ISOLDE are presented in Sec. II. In Sec. III,

*Present address: VITO, IMS, Mol, Belgium.
†Corresponding author. E-mail: piet.vanduppen@fys.kuleuven.ac.be

TABLE I. Overview of the different experimental conditions: total measuring time (Δt), implantation and decay times, and production rate. After experiment II the proton-neutron convertor was found to be twisted, which explains the lower production rate during this experiment. The production rate of gallium was one order of magnitude larger in the case of mass 74, two orders in the case of 76, and more then four orders in the case of mass 78. In a separate experiment, in which the β-delayed neutron decay of ^{78}Cu was measured and the proton beam was impinging on the target, a production rate of $\sim$200 at./μC was obtained [17,18].

^{A}Cu	Δt	Beam on/off (s)	P (at./μC)	Experiment
74	5828 s	0.15/7.25	6 10^5	I
	1980 s	0.2/2.2	6 10^5	I
76	6271 s	0.5/1.6	2 10^4	I
78	403 m	0.4/1.2	0.6	II

the shell-model calculations of even-mass Cu isotopes are presented and the ground-state spin and parity is compared to the experimental data. The systematics of the level schemes of the even-even Zn isotopes is also discussed in that section.

II. RESULTS

A. Experimental setup

The copper isotopes were produced via proton- and neutron-induced fission of ^{238}U at the ISOLDE facility [14]. Two types of production mechanisms were used: the 1 GeV proton beam impinged directly on a standard uranium carbide target of 50 g/cm^2 thickness (labeled exp. I) or it was sent to a tantalum proton-to-neutron converter to induce fission with the low-energy neutrons in order to reduce high-energy proton-induced fission products (labeled exp. II) [15]. The isotopes were subsequently selectively ionized in the laser ion source [16], accelerated to 60 keV, mass separated, and sent to the experimental setup.

The decay-spectroscopy setup consisted of a tape in which the copper isotopes were implanted and which was surrounded by three plastic ΔE detectors for β detection. Two HPGe detectors [64% and 75% (exp. I) or 75% and 90% (exp. II) relative efficiency] were installed in close geometry for γ detection. Singles and list-mode (γ-γ-t and β-γ-t) data were collected. More experimental details on the radioactive beam production and the β-γ detection setup can be found in [1,2].

Different experimental conditions were used during the measuring campaign. The most essential parameters such as production rates, measuring times, and the times of the implantation-decay cycle are summarized in Table I.

B. β decay of ^{74}Cu

In the literature, there is only one decay study on ^{74}Cu, reported by Winger *et al*. [19]. The most accurate half-life value was obtained by Kratz *et al*. [20] by monitoring the β-delayed neutron activity. Reports on reaction studies, probing excited states in the ^{74}Zn-daughter nucleus, are limited. Only a few excited states have been reported, using the ^{76}Ge(^{14}C,^{16}O) and ^{76}Ge(^{18}O,^{20}Ne) reactions [21,22].

The data set on ^{74}Cu consists of decay data taken with the laser switched both on and off. Figure 1 shows a representative part of the singles γ-ray spectra, taken with the 64% relative efficiency detector on mass $A = 74$. A spectrum taken with the lasers switched on (on-resonance) is compared with one taken with the lasers switched off (off-resonance). The measuring time for both spectra is nearly the same (1980 s on- and 2100 s off-resonance). However, the two spectra show some differences because the off-resonance spectrum was taken $\sim$24 h later than the on-resonance spectrum; and in between those spectra, measurements on other mass chains were performed. A major part of the γ lines observed in the off-resonance spectrum are from the decay of surface ionized ^{74}Ga. The ^{74}Ga decay scheme is well known [23], and the most intense lines could be identified in the on- and off-resonance spectra. They are indicated with a star in the figure. To find the laser-enhanced lines, the difference of the two spectra was taken, and this is the bottom spectrum shown in each panel in Fig. 1. For the subtraction, the off-resonance spectrum was rescaled to subtract the ^{74}Ga activity to zero. The multiplication factor was taken from the ratio of the intense 868 keV transition from ^{74}Ga and was found to be 5.1(1). Since this factor is significantly greater than 1, it follows that gallium is produced both in off-resonance, via surface ionization, and in on-resonance, via the ^{74}Cu decay chain. The subtracted spectrum is negative in some regions. To plot the spectrum on a logarithmic scale, a constant (5000) was added to get a positive continuous background. The remaining γ transitions are related to the laser ionization and, therefore, to the ^{74}Cu decay and the ^{74}Zn daughter activity. They are labeled with a number in the figure and are listed in Table II. Only these resonant lines will be considered further.

The peak areas from the β-gated on-resonance spectra are included in Table II and are compared with the peak areas from the off-resonance β-gated spectra. Also shown in the table are the extracted half-life values of the individual γ rays, and the coincident γ-rays. The former were derived by fitting the background-subtracted time spectra with a single-component exponential decay function. The decay time of the data set used is 7.25 s and allows the observation of the γ-intensity variation over a few ^{74}Cu half-lives, $T_{1/2}(^{74}\mathrm{Cu}) = 1.594(10)$ s from [23]. However, some γ rays are doublets with background lines, and for them the background subtraction method will not remove all of the background activity, which is mainly long-lived ^{74}Ga [$T_{1/2}(^{74}\mathrm{Ga}) = 8.1$ min]. For these transitions, it is necessary to make an exponential decay fit on a constant background. Because of the short decay time, this drastically increases the error on the fit parameters. The coincident γ rays were found by making γ-ray gated spectra, using a proper background-subtraction method and a prompt γ-γ-TAC (Time to Amplitude Convertor) condition.

The γ rays with labels 1–5, 10, and 13 all exhibit a longer half-life. They are known to come from the ^{74}Zn daughter nucleus, which has a 95.6(12) s half-life [23]. As the period during which the decay was observed is only 7.25 s, the γ-ray intensity is almost constant and the observed half-lives of these γ rays do not agree with the ^{74}Zn half-life. One does also

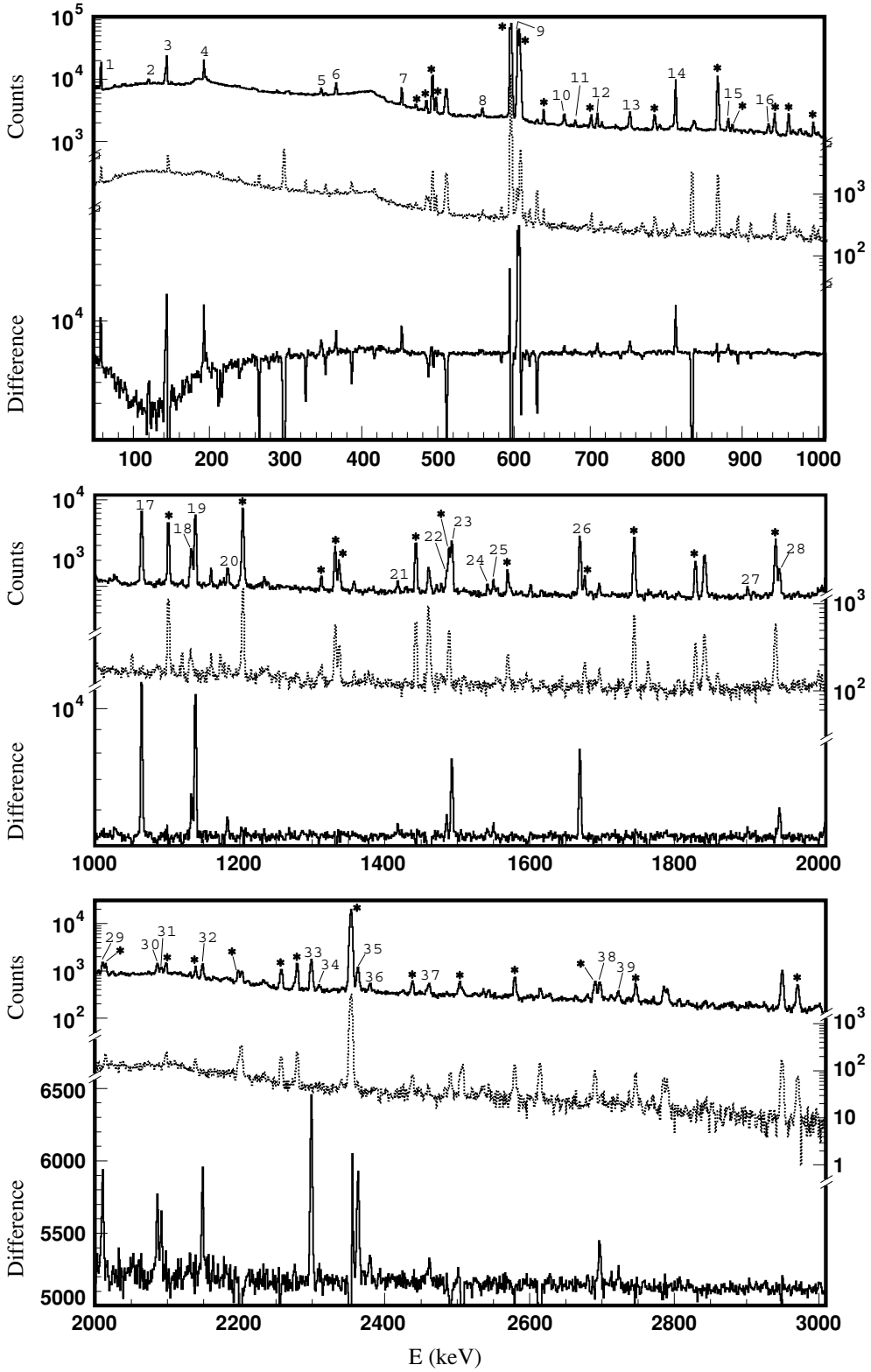

FIG. 1. Part of the singles spectra with lasers switched on (top and left scale) and off (middle and right scale) taken with the 64% relative efficiency detector on mass $A = 74$. Not all statistics are shown. The bottom spectrum (lower left scale) is the difference between the on-resonance and the rescaled off-resonance spectrum and a constant of 5000 is added (see text). The lines labeled with a number are enhanced in the on-resonance spectrum and are listed in Table II. Lines labeled with a star are from surface-ionized ^{74}Ga.

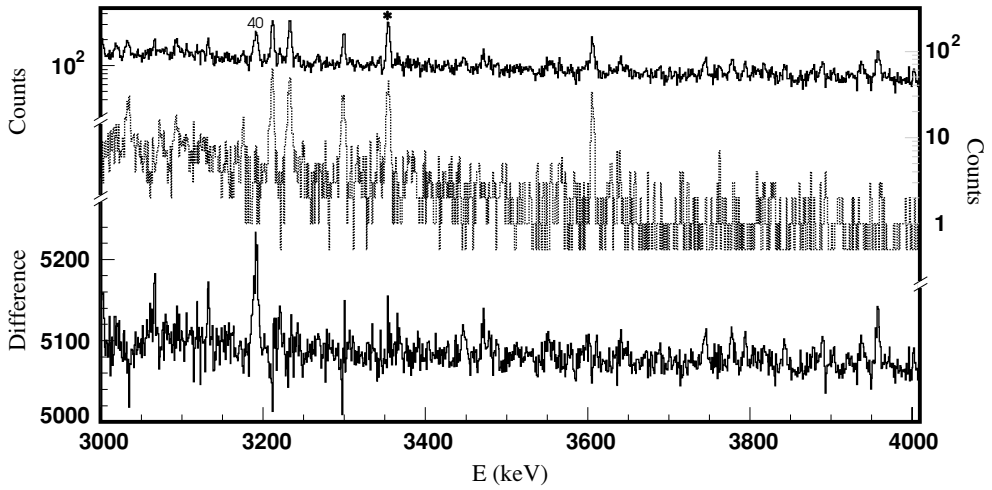

FIG. 1. (*Continued*.)

observe that some of the ^{74}Zn γ rays are mutually coincident, according to the known decay scheme [23]. Note that the 56.7 keV transition is populated by a decaying isomeric state in ^{74}Ga at 59.8 keV that has a 9.5(10) s half-life.

All other γ rays exhibit a half-life that agrees with the 1.594(10) s ^{74}Cu half-life. Moreover, the coincidence relations between the γ rays also show that all these γ rays belong to the same decay scheme and thus to the β decay of ^{74}Cu. Notice that some lines are doublet lines with nonresonant ^{74}Ga background, like the 1133, 1183, and 1487 keV transitions. For them, the background cannot be removed completely from the peak area. Therefore, they also show coincidences with ^{74}Ga transitions: the 493, 596, 608, 1101, 1135, 1204, 1489, 1941, and 2098 keV γ rays from ^{74}Ga are observed in the γ-ray gated spectra of the 1133, 1183, and 1487 keV transitions. Notice that the 1489 keV transition from gallium is distinct from the 1487 keV transition from ^{74}Cu. In ^{74}Ga, the 1489 keV γ ray is coincident with the 1135 keV γ ray and forms a doublet with the 1133 keV γ ray from ^{74}Cu. Therefore, the 1133 and 1487 keV lines from ^{74}Cu appear to be coincident. In reality, however, both γ rays are doublets, and the observed coincidence relation comes from the existing coincidence in the gallium background.

Thus, we can state that all γ rays from Table II are from either the β decay of ^{74}Zn (lines 1–5, 10, and 13) or the β decay of ^{74}Cu. This is based on the half-life and coincidence relations of the resonant γ rays. From the half-life values, there is no indication of the existence of a second β-decaying isomer in ^{74}Cu. No laser frequency scan measurements were done on this isotope, but we will further assume only one decaying isomer [9].

From the coincidence relations from Table II, a decay scheme for the β decay of ^{74}Cu can be constructed. The result is shown in Fig. 2. Most of the γ rays could be placed unambiguously. Only the 1133 keV γ ray has unexpected coincidence relations: because of the energy match and the coincidences with the 606, 813, 1419, and 2011 keV γ rays, the γ ray is likely to come from the 2552 keV level. But the transition appears to be coincident with the 1065 and 1671 keV lines as well. However, the coincidence with the 1065 and 1671 keV γ rays is weak and can be understood because the 1133 keV line is a doublet with the 1139 keV line. The latter is clearly coincident with the 1065 and 1671 keV γ rays, and hence the observed coincidences with the 1133 keV line are artificial.

The true summing contribution for cross-over transitions is estimated. Only the 1419 keV transition is a true summing line of the two most intense 606 and 813 keV γ rays. The transition is therefore not included in the decay scheme.

The γ-ray intensities are calculated from the efficiency-corrected β-gated peak areas from Table II. The off-resonance peak areas, also in Table II, are subtracted, and cross-over transitions are corrected for summing. The γ-ray intensities, normalized to the most intense γ ray, are summarized in Table III. These values are used to deduce the β-branching ratios to the excited states in ^{74}Zn. The β feeding to the ground state could not be determined experimentally, but from spin considerations it is expected to be small (see below). Therefore, the β- and γ-ray branching ratios shown in Fig. 2 are normalized to the total γ decay, i.e., the intensity of the γ-ray transitions arriving at the ground state sums up to 100. The log ft values are calculated assuming no β feeding to the ground state. The quoted Q_β value is taken from [24]. Levels that are already known in the literature [24] are labeled with x in Fig. 2.

The decay scheme obtained from the decay study of Winger *et al*. [19] is less elaborate than ours, but all levels from Winger *et al*. are also present in our decay scheme, except for the 1164 and 2616 keV levels. The level at 1164 keV is an intermediate level in a 505 to 558 keV γ-ray cascade populating the 606 keV state. It was established by Winger *et al*. because of the observed coincidence between these two transitions and because the energy of the cascade sums up to 1670 keV, a well-established level. However, our data set has 30 to 40 times better statistics and no 505 keV γ ray is observed. Furthermore, the 558 keV is clearly coincident with the 1493 keV transition, and therefore we do not confirm the existence of the 1164 keV level. The same holds for the level at 2616 keV. This level was proposed because of the 2011 and 517 keV depopulating γ rays. In our data, no 517 keV γ ray is observed, and the

TABLE II. Energy values, peak areas from the on- (A_{on}) and off-resonance (A_{off}) β-gated spectra, half-life values, and coincident γ rays of the resonant lines at $A = 74$ shown in Fig. 1. For the coincident γ rays the peak areas are shown in brackets.

Label	E (keV)	A_{on}	A_{off}	$T_{1/2}$ (s)	Coincident γ rays
1	56.7(4)	525(111)	–	10(2)	–
2	119.6(4)	549(110)	–	12(2)	666(47)
3	143.2(4)	6454(166)	111(45)	15(6)	753(161)
4	192.5(4)	4017(145)	–	15(2)	–
5	346.7(5)	670(111)	–	12(2)	–
6	366.4(5)	2018(115)	–	1.8(4)	606(126), 2092(55), 2698(70)
7	452.52(9)	2745(99)	–	1.6(2)	606(365), 681(27), 813(20), 1493(154), 2011(30)
8	558.5(6)	687(64)	–	0.8(11)	606(150), 1493(60)
9	606.01(5)	57341(212)	378(20)	1.72(5)	366(126), 453(381), 559(178), 681(110), 710(155), 813(1239), 882(140), 935(83), 1064(1657), 1133(259), 1139(716), 1183(160), 1487(50), 1493(400), 1543(53), 1551(70), 1946(190), 2011(116), 2086(94), 2092(68), 2299(369), 2363(200), 2380(43), 2461(60), 2723(40), 3191(15)
10	666.4(7)	375(69)	–	10(2)	120(24)
11	680.8(7)	230(65)	–	2.0(15)	606(73), 813(44)
12	709.7(7)	958(58)	–	0.9(11)	606(195), 1493(113)
13	752.9(7)	521(64)	–	11(2)	143(64)
14	812.6(1)	5963(95)	–	1.65(7)	606(1274), 681(52), 935(77), 1133(160), 1487(97), 1551(67), 2011(33)
15	881.9(8)	768(57)	–	1.0(2)	606(80), 1064(38), 1671(28)
16	935.0(9)	408(45)	–	1.9(17)	606(70), 813(62)
17	1064.4(1)	6578(93)	–	1.68(6)	606(1636), 882(60), 1139(444), 1901(20), 2086(30), 3191(10)
18	1133(1)	1552(55)	39(11)	0.9(7)	493(60), 596(277), 606(247), 813(164), 1064(19), 1101(58), 1204(52), 1419(10), 1489(44), 1671(16), 2011(25), 2098(15)
19	1139(1)	5772(87)	–	1.63(7)	606(679), 1064(466), 1671(332), 2086(60)
20	1183(1)	462(47)	32(13)	3(97)	596(35), 606(138), 1941(16)
21	1419(1)	297(38)	–	2(5)	1133(12)
22	1487(1)	599(41)	–	4(2)	596(30), 606(70), 608(60),813(79), 1135(12), 1204(24), 1419(5)
23	1493(1)	2846(69)	35(15)	1.8(1)	453(158), 559(65), 606(363), 710(115), 2011(17)
24	1543(1)	194(36)	–	2(6)	606(50)
25	1551(1)	361(39)	–	1(3)	606(80), 813(52)
26	1670.7(9)	3235(74)	–	1.9(1)	882(36), 1139(319), 1901(17), 2086(20), 3191(14)
27	1901(5)	269(46)	–	3(3)	606(43), 1064(22), 1671(17)
28	1946(2)	980(84)	–	2.3(5)	606(194), 2011(30)
29	2011(2)	762(79)	–	1.0(2)	453(26), 606(120), 813(30), 1133(15), 1493(18), 1946(22)
30	2086(2)	559(43)	–	2(3)	606(79), 1064(41), 1139(48), 1493(6), 1671(25)
31	2092(2)	320(38)	–	3(2)	366(40), 606(85)
32	2149(2)	756(46)	–	1(2)	–
33	2299.1(3)	1765(53)	–	1.6(1)	606(336)
34	2310(2)	166(29)	–	1(3)	606(17), 813(3), 1133(4)
35	2363(2)	862(42)	–	1.8(4)	606(191)
36	2380(2)	185(32)	–	1.1(9)	606(67)
37	2461(3)	241(30)	–	4(2)	606(55)
38	2698(3)	333(27)	–	1.8(5)	366(61)
39	2723(3)	151(32)	–	1.1(16)	606(35), 813(6), 1487(7), 1493(4),2299(14)
40	3191(4)	223(22)	–	2(1)	606(24), 1064(10), 1671(12)

2011 keV γ ray shows several clear coincidence relations with the γ rays from the 2552 keV level. Hence, it is placed on top of this level, and the 2616 keV level is not existing in our decay scheme. Therefore, the 1164 and 2616 keV levels from [19] are omitted.

Spin-parity assignments shown in Fig. 2 are taken primarily from the β-decay study of Winger *et al.* [19]. The level at 1419 keV was proposed by Winger *et al.* to have spin-parity of 0^+ or 4^+ since no γ ray was feeding the 0^+ ground state. In our data, a possible ground-state transition of 1419 keV was observed, but it was shown to be a sum peak. Therefore, the $(0^+,4^+)$ assignments are still valid. Furthermore, we note that several other levels, the 2099, 2552, 2905, and 2970 keV, are decaying to the 606 and 1419 keV states, but none of them decays to the 0^+ ground state. If the 1419 keV state would have $I^\pi = 0^+$, we would expect these states to also decay to the 0^+ ground state. The observed feeding pattern could then only be explained by assuming that the 0^+ ground state and the supposedly 0^+ state at 1419 keV have different shell-model configurations. If, on the other hand, the 1419 keV state has

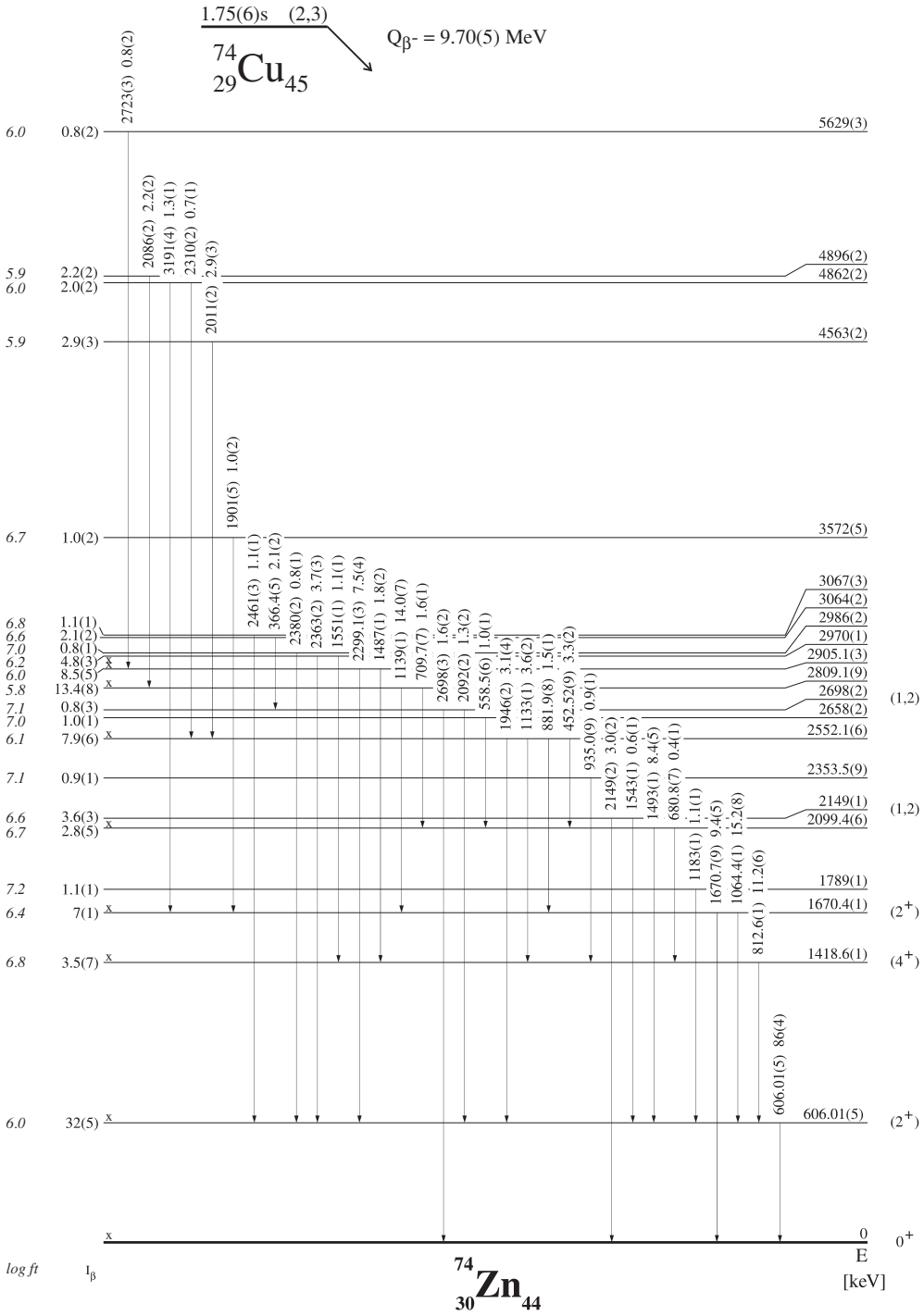

FIG. 2. Deduced decay scheme for ^{74}Cu. Log ft should be considered as lower limits. Levels labeled x are known from the literature [24], and the Q value was taken from [30].

$I^\pi = 4^+$, no decay from the above states to the 0^+ ground state is expected and the observed feeding pattern is accounted for. We opt for the second, most plausible assumption and assign a tentative spin parity of 4^+ to the 1419 keV level.

The state at 1670 keV was assigned a tentative spin parity of (2^+) by Winger *et al*. since it decays both to the 2_1^+ at 606 keV and the 0^+ ground-state. A spin 1 is also possible, but from systematics it is more likely to be the 2_2^+ state. We therefore adopt the tentative 2^+ spin-parity assignment. Note that the strongly populated level at 2809 keV decays to this (2_2^+) level but not to the 2_1^+ at 606 keV. It suggests that the two 2^+ states have different configurations.

On the same basis, we can further argue that the 2149 and 2698 keV states will have spin 1 or 2 because both states decay to the 0^+ ground-state and the 2_1^+ excited states.

TABLE III. Relative γ-ray intensities (I_{rel}) from the β decay of ^{74}Cu. The values are normalized so that the most intense γ-ray transition has $I_{rel} = 100$.

E (keV)	I_{rel}	E (keV)	I_{rel}
366.4(5)	2.4(2)	1551(1)	1.3(2)
452.52(9)	3.9(2)	1670.7(9)	10.9(6)
558.5(6)	1.1(1)	1901(5)	1.1(2)
606.01(5)	100(5)	1946(2)	3.6(4)
680.8(7)	0.4(1)	2011(2)	3.4(4)
709.7(7)	1.9(1)	2086(2)	2.6(2)
812.6(1)	13.1(7)	2092(2)	1.5(2)
881.9(8)	1.8(2)	2149(2)	3.5(3)
935.0(9)	1.0(1)	2299.1(3)	8.7(5)
1064.4(1)	17.6(9)	2310(2)	0.8(2)
1133(1)	4.2(3)	2363(2)	4.3(3)
1139(1)	16.3(9)	2380(2)	1.0(2)
1183(1)	1.2(2)	2461(3)	1.3(2)
1487(1)	2.1(2)	2698(3)	1.8(2)
1493(1)	9.7(5)	2723(3)	0.9(2)
1543(1)	0.7(1)	3191(4)	1.5(2)

Concerning the spin and parity of ^{74}Cu, we observe that the levels not decaying directly to the ^{74}Zn ground-state are receiving a substantial amount of β feeding: 56.8% in total. It shows that ^{74}Cu is likely to have a spin larger than 1. For if it were 0 or 1, only states up to spin 2 would get strong feeding and these can decay directly to the ground-state. Because the 2_1^+ still has a log ft of 6.0 (although this should be considered as a lower limit because of γ transitions from higher lying levels that may not have been detected), we propose a spin of 2 or 3 for the ^{74}Cu mother. As a consequence, the β feeding to the 0^+ ground-state in ^{74}Zn will be close to zero. Winger *et al.* proposed a spin-parity of 1^+ or 3^+ for ^{74}Cu because of the strong β feeding to the level at 1419 keV, which was supposed a 0^+ or 4^+ state (see above). The positive parity was assumed because of the systematics in odd-A nuclei.

The ^{74}Cu half-life was determined using two carefully selected γ rays. The γ-ray spectra were produced with gate settings on time slices in the 7.25 s decay part of the time spectrum. The peak areas of the ^{74}Cu γ rays can then be determined as a function of time. The most intense 606 keV γ ray was not used because it is a doublet with the 608 keV from ^{74}Ga which has a 8.12 min half-life. Other intense lines are the 813, 1064, 1139, 1493, and 1671 keV transitions, but the latter three are also doublets and are therefore not used. The 813 and 1064 keV transitions appear to be pure and single ^{74}Cu lines (see Fig. 1). Their peak areas as a function of time are shown in Fig. 3. Also shown in the figure are the peak areas for the 596 keV transition of ^{74}Ga. Since this isotope has a long half-life ($T_{1/2} = 8.12$ min) compared to the measuring cycle (7.25 s), its activity should be nearly constant. Hence, monitoring the 596 keV peak areas is a way to monitor the dead time of the detectors and the data-acquisition system. Since the

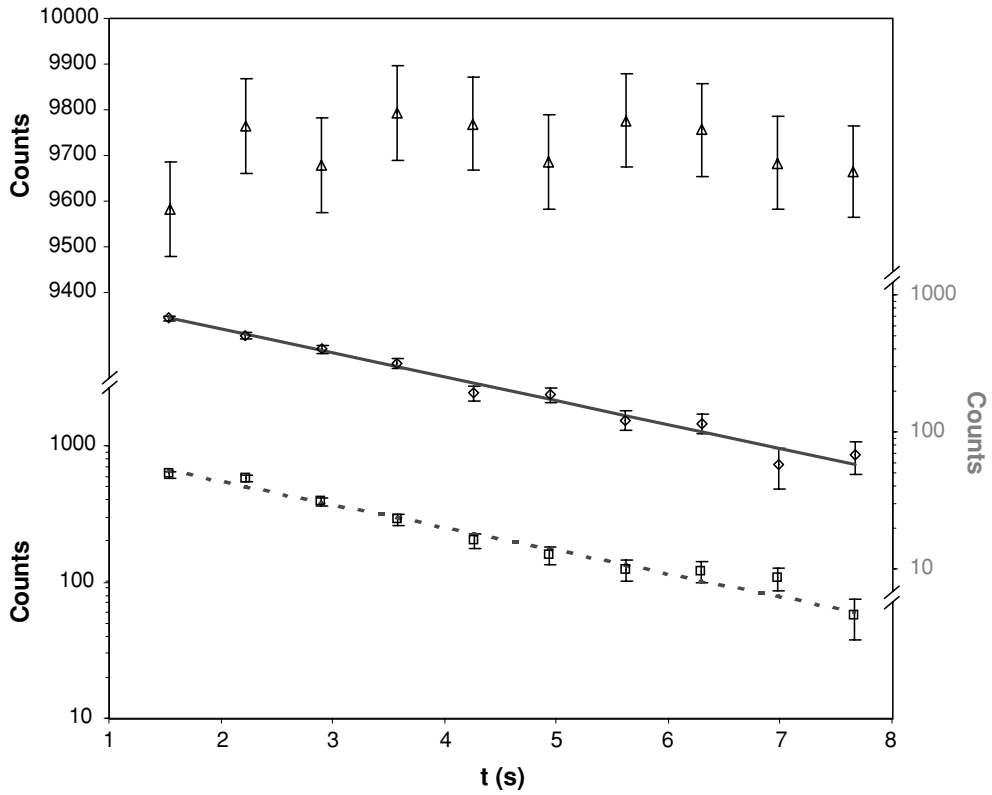

FIG. 3. Peak areas of the 813 (squares, lower left scale), 1064 (diamonds, right scale) and 596 keV (triangles, top left scale) transitions for gates on different time slices in the time spectrum. The solid and dotted lines represent exponential fits to the data. The 596 keV γ ray from ^{74}Ga is used to monitor the dead time of the system.

596 keV peak areas remain constant, to within the ∼1% error, dead-time effects can be neglected. The 813 and 1064 keV peak areas from ^{74}Cu were fitted with a single-component exponential decay function: $y = A_1 e^{-t/t_1}$ and yield half-life values of 1.78(9) and 1.72(9) s, respectively. To rule out possible background components, the same data were fitted with the fit function including a constant background. No indications of a background component in any of the two peaks were found. As final value for the ^{74}Cu half-life, we therefore adopt the mean value of the above half-lives, yielding $T_{1/2} = 1.75(6)$ s. Our value deviates slightly from the literature value [1.594(10) s] [20]. The latter was obtained by measuring the time dependence of β-delayed neutrons coming from the decay of ^{74}Cu. A possible explanation for a deviation can be that the radioactive beam in the previous experiment was contaminated with doubly charged ions or molecular ions containing other neutron emitters. In the present work, resonant laser ionization was used, to reach a cleaner, more selective condition. A careful examination of the spectra did not show a clear signature of γ radiation from the deexcitation of excited states in ^{73}Zn.

C. β decay of ^{76}Cu

What is known about ^{76}Cu comes primarily from the β-decay study of Winger *et al*. [25]. This group proposed the existence of a second isomer in ^{76}Cu [with $T_{1/2} = 1.27(30)$ s], but so far, no other experimental work has been able to confirm this. The most accurate half-life value for the ^{76}Cu ground state was determined by Kratz *et al*. [20] to be $T_{1/2} = 641(6)$ ms. No excited states in the ^{76}Zn-daughter nucleus were observed using methods other than β decay of ^{76}Cu.

The data set for ^{76}Cu consists of decay data taken with the laser switched on and off. Figure 4 shows part of the on- and off-resonance singles spectra, taken with the 64% relative efficiency germanium detector on mass $A = 76$. The measuring time for the on-resonance spectrum is 6271 s and 2321 s for the off-resonance spectrum, but the implantation times were changed during the measurements. Most of the activity observed in the spectra is nonresonant, coming from surface-ionized ^{76}Ga. The ^{76}Ga decay scheme is well known [23], and the most intense lines could be identified in the on- and off-resonance spectra. They are indicated with a star in the figure. There are, however, also a number of laser-enhanced lines, which are labeled with a number in Fig. 4 and listed in Table IV. They are related to the ^{76}Cu decay and daughter activity. Only these resonant lines will be considered further.

Peak properties are summarized in Table IV. Peak areas are taken from the β-gated on- and off-resonance spectra. The half-lives are derived from a single-component exponential decay fit of the time-dependent γ-ray intensities, obtained from projecting the γ-ray spectrum with different gate settings on the time spectrum of the coincidence data. The decay period of the used data file is 1.6 s, and this allows the observation of the decay for a few ^{76}Cu half-lives, $T_{1/2} = 0.641(6)$ s from [20]. In [25], a second half-life of 1.27(30) s is reported and claimed to come from a second isomer in ^{76}Cu. In our data, there is no sign of a second half-life (see below). The ^{76}Zn daughter has a 5.6 s half-life value, and thus its γ ray intensity will have a nearly flat time dependence in the 1.6 s time spectrum. Coincidence relations are derived from background-subtracted γ ray gated spectra with a prompt TAC condition.

The γ rays with labels 1, 2, 4, 6, 14, and 15 cannot be fitted with a single-component exponential fit. They are known to come from the β decay of the ^{76}Zn daughter nucleus and the negative half-life represents the production of ^{76}Zn coming from the ^{76}Cu mother decay. The γ rays with labels 7 and 9 are also known ^{76}Zn β-decay lines, and coincidences are indeed observed with the other ^{76}Zn lines. Furthermore, most of these lines show mutual coincidences and in some coincidence gates new γ rays are observed. Note that the 172 keV transition (label 2) show no coincidence with any other known γ ray from ^{76}Zn. However, the coincidence with a 103 keV line indicates a relation with $275 = 103 + 172$ keV, an energy which matches the 275 keV γ ray. Therefore, and because of the half-life, it is likely to come from ^{76}Zn. Hence, we can safely assign all the above-mentioned eight γ rays to the ^{76}Zn decay. The other γ rays from Table IV exhibit a short half-life, in agreement with the 0.641(6) s ^{76}Cu half-life. They show mutual coincidences, and therefore we can attribute all these γ rays to the decay of ^{76}Cu. Based on the 599 and 698 keV half-life behavior, there is no indication of a second longer-lived isomer in our data. Since there is no immediate sign coming from the half-life values of the other γ rays from Table IV, no further support for the existence of a second isomer is found.

A decay scheme for ^{76}Cu could be constructed from the coincidence relations in Table IV. It is shown in Fig. 5. All γ rays could be placed unambiguously except for the 464, 1053 and 1296 keV γ-rays. The intensities of the 464 and 1053 keV transitions suggest that the order of these γ rays in cascade might as well be reversed, defining a level at 1761 instead of 2349 keV. The same uncertainty existed in the work of Winger *et al*. [25], see below. Therefore, the level and both transitions are drawn with dashed lines. Note also that the weak γ rays observed in the γ-ray gated spectra at 1517, 1937, and 2375 keV could be placed based on their coincidence relations and the correct energy match between existing levels. The 1296 keV transition is not placed because it appears to be a pure summing line. All other bypassing transitions are real transitions.

The γ-ray intensities are calculated from the β-gated peak areas from Table IV. They are corrected for the off-resonance peak area taking into account the different time cycle, the summing contribution in case of a cross-over transition, and the detection efficiency. The γ-ray intensities, normalized to the most intense γ ray, are summarized in Table V. These values are used to deduce the β-branching ratios to the excited states in ^{76}Zn. The β feeding to the ground state could not be determined experimentally, but from I^π considerations it is expected to be small (see below). Therefore, the β- and γ-ray branching ratios shown in Fig. 5 are normalized to the total γ decay, i.e., the intensity of γ rays arriving at the ground state sums up to 100. The log ft values are calculated assuming no β feeding to the ground state. The quoted Q_β value is taken from [26]. Levels already known in literature [26] are labeled with x in Fig. 5.

The ^{76}Cu decay scheme from Winger *et al*. [25] compares well with the one from this work, though there are several

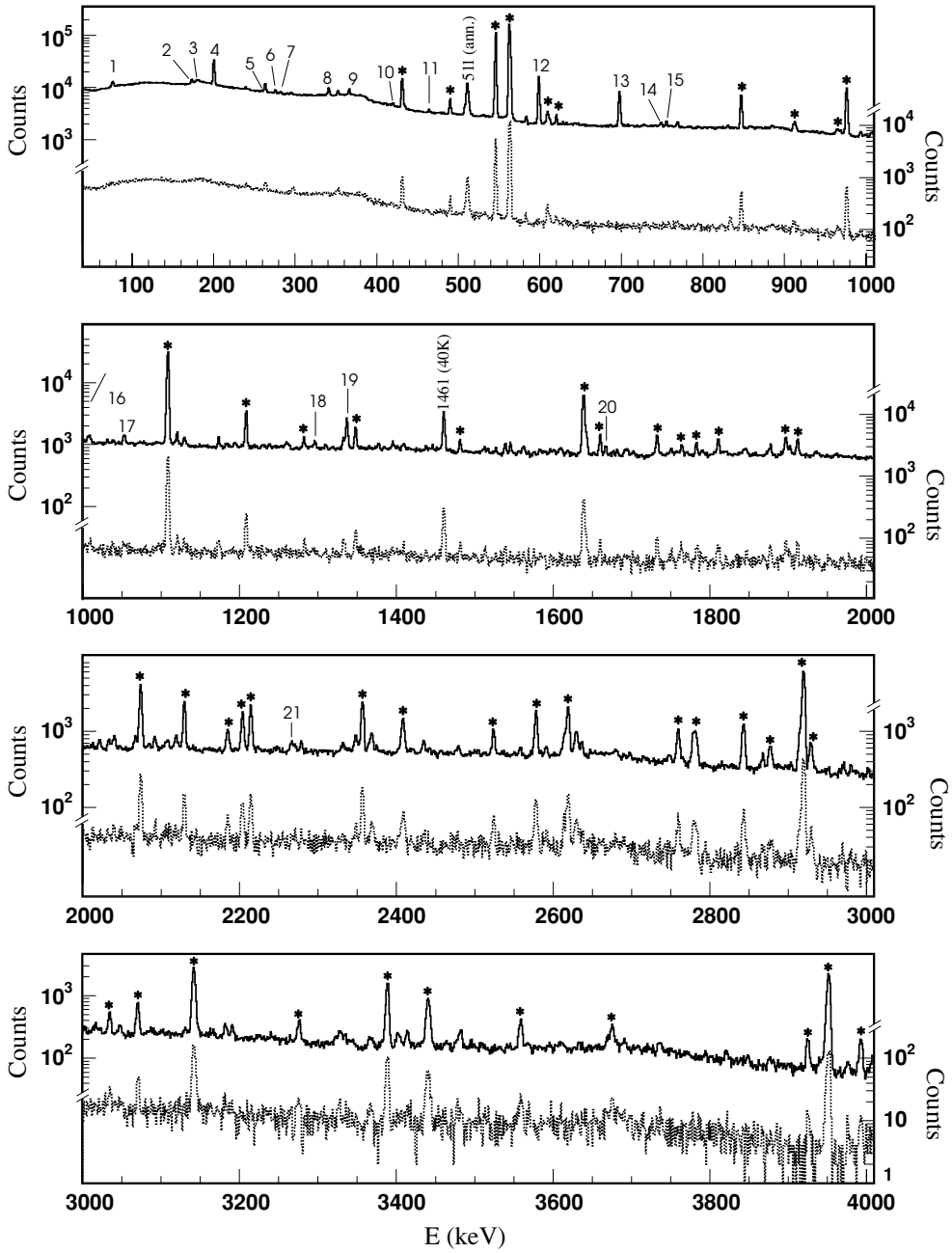

FIG. 4. Part of the singles spectra with lasers switched on (black, left scale) and off (grey, right scale) taken with the 64% relative efficiency detector on mass $A = 76$. The lines labeled with a number are enhanced in the on-resonance spectrum and listed in Table IV. Lines labeled with a star are from surface-ionized ^{76}Ga.

differences. First, as mentioned above, an ambiguity exists in both schemes about the order of the γ rays in the 464–1053 keV cascade. Winger *et al*. proposed the 1053 keV γ ray as being the upper γ ray in the cascade, defining the intermediate level at 1761 keV. Because of the slightly larger intensity of the 1053 keV γ ray in this work, we propose the opposite order, defining the intermediate level at 2349 keV. Second, the levels at 1031 and 1716 keV from [25] conflict with our observations. The 1031 keV level was established because it is an intermediate level in the 1783–432 keV γ-ray cascade, originating from the 2814 keV level. Both γ rays are present in the spectra from this work, shown in Fig. 4, but they were attributed to the decay of ^{76}Ga since none of them showed an enhancement induced by the lasers. Furthermore, both γ rays were found to be coincident only with other ^{76}Ga γ-rays, confirming their ^{76}Ga origin. Hence, the 1031 keV state is omitted. The level at 1716 keV was established based on the 1098–419 keV γ-ray cascade, originating from the same 2814 keV level. No 1098 keV γ ray was observed in our spectra. The 419 keV γ ray could be attributed to the decay

TABLE IV. Energy values, peak areas from the on- (A_{on}) and off-resonance (A_{off}) β-gated spectra, half-life values, and coincident γ rays (peak areas are shown in parentheses) of the resonant lines at $A = 76$ shown in Fig. 4.

Label	E (keV)	A_{on}	A_{off}	$T_{1/2}$ (s)	Coincident γ rays
1	75.3(2)	1653(120)	–	–	200(100), 755(10)
2	172.3(3)	1186(129)	–	–	103(25), 509(21), 857(28)
3	179.6(3)	1060(93)	–	1.7(10)	419(51), 599(12), 698(30), 1337(13)
4	199.5(3)	13512(217)	–	–	75(100), 366(100), 755(31), 831(25)
5	258.5(1)	428(85)	–	0.5(9)	341(19), 599(15), 698(24)
6	275.4(3)	821(136)	–	–	290(30), 755(20)
7	281.5(4)	299(112)	–	1(10)	749(22), 1264(14)
8	340.87(9)	2767(110)	–	0.6(7)	259(20), 599(133), 698(147), 1337(91)
9	365.8(4)	1387(144)	123(76)	3(4)	200(84)
10	419.3(4)	512(62)	–	0.4(7)	180(45), 464(23), 599(16), 698(23), 1053(15), 1337(10), 1517(11)
11	464.3(3)	410(54)	–	0.6(5)	419(35), 599(40), 698(16), 1053(20)
12	598.70(6)	11559(121)	55(36)	0.63(3)	341(154), 419(38), 464(55), 599(30), 698(365), 1007(10), 1053(14), 1337(117), 1668(16), 2375(17)
13	697.69(7)	6058(92)	–	0.67(4)	180(26), 341(157), 419(38), 464(25), 599(812), 1053(25), 1337(204), 1937(12)
14	749(1)	240(68)	–	–	82(6), 200(17), 282(34)
15	755(1)	271(55)	–	–	75(12), 200(27), 275(21)
16	1006.5(2)	391(49)	117(29)	0.9(5)	366(16), 563(60), 599(26), 1348(20), 1668(7)
17	1053(1)	395(39)	76(23)	0.7(2)	419(20), 464(15), 599(23), 698(16)
18	1296.2(2)	228(33)	–	0.4(7)	341(9), 1337(20)
19	1337(1)	1859(57)	–	0.7(1)	180(14), 341(100), 599(230), 698(211), 1296(24)
20	1668(2)	180(32)	–	0.9(5)	599(20)
21	2266(3)	146(26)	–	0.5(7)	1007(7)

of ^{76}Cu but was connected to the 3233 keV level based on solid coincidence relations with other ^{76}Cu γ rays. Hence, the 1716 keV level is also omitted.

Tentative spin-parity assignments of the ^{76}Zn levels are primarily taken from Winger *et al*. [25]. The (2^+) assignment to the 599 keV level from Winger *et al*. was mainly based on systematics. The I^π assignment of the 1296 keV level was based on the observation of the 341–1337–698–599 keV γ-ray cascade, which gets a considerable amount of feeding. Because similar cascades are observed in the ^{68,70}Cu decay and because in each case the state above the 2^+ state was assigned 4^+, they postulated the 1296 keV level to have $I^\pi = (4^+)$.

We will adopt the (2^+) assignment for the 599 keV level. For the 1296 keV level, we can argue that this level is decaying only to the (2^+) state and not to the 0^+ ground state. Therefore its I^π is most likely 0^+ or 4^+. Since most of the states above the 2266 keV level decay in one or more steps to the 1296 keV level and not directly to the 0^+ and 2^+ states, it indicates that the spin of these levels is larger than 2 and, with this, that the 1296 keV level is most probably the 4^+ state instead of the 0^+ state. In particular, the above-mentioned intense γ-ray cascade is observed in our decay scheme as well and just like in [25]; this supports the $I^\pi = (4^+)$ assumption. This $I^\pi = (4^+)$ assignment further restricts the spin of the 2266 keV level to 1 or 2 since this level only decays to the 0^+ and (2^+) states and not to the 1296 keV state.

The ^{76}Cu mother decays primarily to the levels at 599, 1296, 2633, and 2974 keV ($\log ft < 6$). Using the above arguments, the 2633 and 2974 keV levels have spins larger than 2, and the 1296 keV level has $I^\pi = (4^+)$. This suggests that the ^{76}Cu mother spin is larger than 2. Note that the $\log ft$ values for the first 4^+ level in ^{72,74}Cu are substantially larger, indicating a lower value for the respective copper mother spins. Furthermore, since there is also significant β feeding to the (2^+) state at 599 keV ($\log ft = 5.8$), we propose spin 3 or 4 for the copper mother. Consequently, the ground-state β feeding will be small.

The determination of the ^{76}Cu half-life was performed by projecting γ-ray spectra with gates on different time slices in the time spectrum of the coincidence data. The used data file was taken during 2300 s and has a total decay period of 1.6 s. The peak areas of the most intense 599 and 698 keV γ rays as a function of time are shown in Fig. 6. Both decay curves are fitted with single-component exponential decay functions: $y = A_1 e^{-t/t_1}$, yielding half-life values of 634(31) and 671(39) ms for the 599 and 698 keV transitions, respectively. To rule out possible background components, the same data were fitted with the fit function including a constant background. No indication of a background component in any of the two peaks was found. Both half-life values agree with the more precise value of 641(6) ms from the β-delayed neutron measurements of Kratz *et al*. [20]. However, they contrast with the observations of Winger *et al*. [25], where the half-lives of the 599 and 698 keV γ rays were found to be 0.84(6) and 0.57(6) s, respectively, suggesting the existence of a second β-decaying isomer. Note that the latter values were derived from a $\sim$1 s time spectrum. While the present work should be more sensitive to the observation of a longer-lived isomer (the period during which the decay was observed was 1.5 s), no difference in half-life of the 599 and 698 keV lines were found, and thus there is no reason to assume a second isomer in ^{76}Cu. Furthermore, a laser scan measurement on mass $A = 76$ was

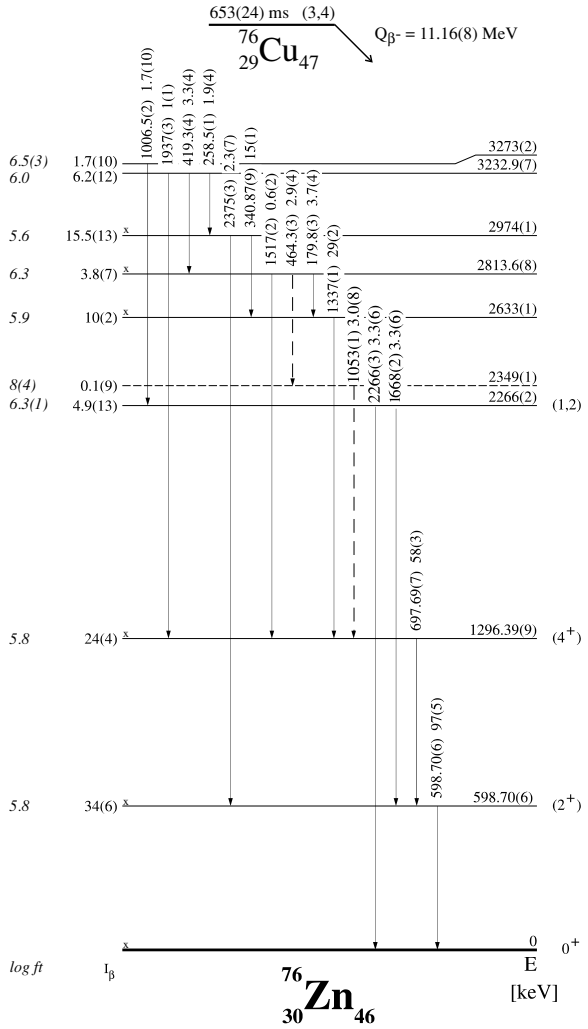

FIG. 5. Deduced decay scheme for ^{76}Cu. Log ft should be considered as lower limits. Levels labelled with x are known from the literature [26], and the Q value was taken from [30].

TABLE V. Relative γ-ray intensities $I_{\rm rel}$ from the β decay of ^{76}Cu. The values are normalized so that the most intense γ-ray transition has $I_{\rm rel} = 100$.

E (keV)	$I_{\rm rel}$
179.6(3)	3.8(4)
258.5(1)	2.0(4)
340.87(9)	16(1)
419.3(4)	3.4(4)
464.3(3)	3.0(4)
598.70(6)	100(5)
697.69(7)	59(3)
1006.5(2)	1.7(10)
1053(1)	3.1(9)
1337(1)	30(2)
1517(2)	0.6(2)
1668(2)	3.4(6)
1937(3)	1.0(11)
2266(3)	3.4(6)
2375(3)	2.3(7)

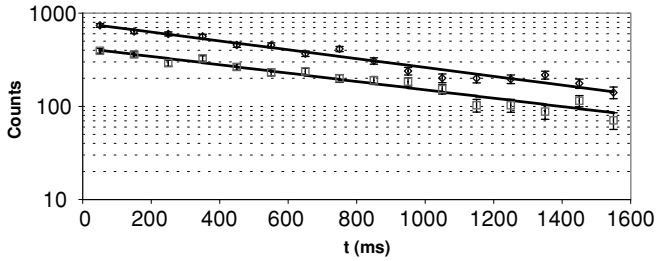

FIG. 6. Peak areas of the 599 (diamonds) and the 698 keV transitions (squares) for gates on different time slices in the time spectrum. The solid lines represent fits to the data using single-component exponential decay functions.

performed to find signs for a possible second isomer [9]. The 599 and 698 keV scan curves show no difference. Hence, we will further assume that only one ^{76}Cu isomer was observed. We take as a final half-life value, the mean value of the two half-life values, yielding 653(24) ms. γ rays coming from the decay of excited states in ^{75}Zn were looked for, but no sign of any γ-rays could be found in the singles spectra or in the β-gated coincidence spectra.

D. β decay of ^{78}Cu

In the literature, only limited data on the ^{78}Cu nucleus exists. Lund *et al.* [27] reported three γ rays observed in the decay of ^{78}Cu, and Kratz *et al.* determined its half-life [20]. Four excited states, including an isomeric state, were reported by Daugas *et al.* [28] in the ^{78}Zn daughter nucleus, produced via a fragmentation reaction.

The data set on ^{78}Cu consists of decay data and was obtained from the experiment in which the proton-to-neutron converter was placed next to the ISOLDE target in order to suppress the rubidium contaminations in the beam. Fig. 7 shows a sample of the on- and off-resonance spectra, taken with the 90% relative efficiency detector on mass $A = 78$. Data were taken for about 7 h on-resonance and 4 h off-resonance. The multiscaling spectra were divided over the implantation-decay cycle in time units of 160 ms each. The spectra shown contain only the first six time units, corresponding to the first 960 ms of the implantation-decay cycle. This way, the short-lived ^{78}Cu activity, $T_{1/2} = 342(11)$ ms [20], is enhanced compared to longer-lived isobaric contaminations. It is evident that the spectra are overwhelmed by nonresonant activity, coming mainly from surface-ionized ^{78}Ga and related ^{78}Ge and ^{78}As daughter activities. Only three weak laser-enhanced lines could be identified. These lines are numbered and listed in Table VI.

The peak areas from the β-gated spectra are shown in Table VI. The 890.7(3) keV transition sits on top of a nonresonant contribution, coming from ^{78}Ga and ^{78}As with transitions of 891.3(16) keV and 888.7(1) keV, respectively [23]. The nonresonant contribution is subtracted, using a scaling factor deduced from the ratio of the gallium activity in on- and off-resonance spectra. The 891.3(16) keV γ ray is the main component underneath the resonant line at 890.7 keV.

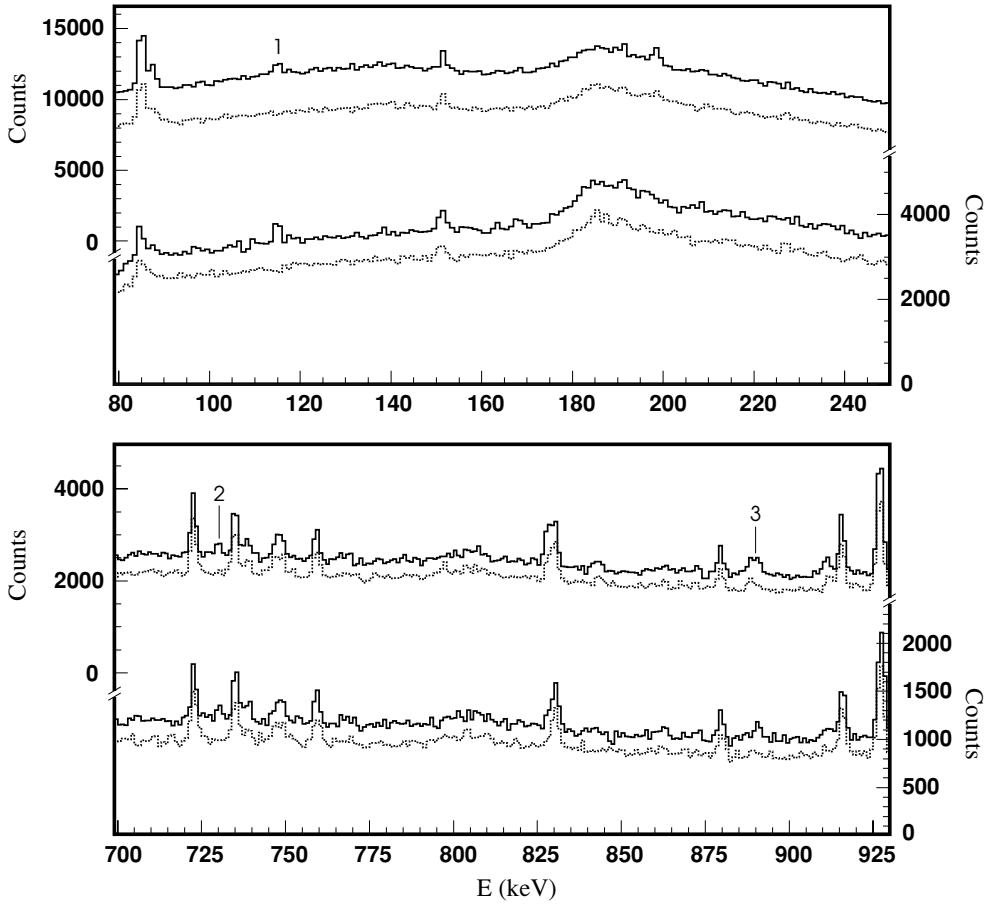

FIG. 7. Part of the multiscaling and β-gated spectra around the three resonant transitions observed at mass 78. The two singles spectra (on- and off-resonance) are shown on top (left scale) of each panel, and the β-gated spectra at the bottom (right scale). On-resonance spectra are black, off-resonance spectra are grey.

The resonant peak areas are then corrected for the detection efficiency and are normalized to the most intense 114.9 keV γ ray.

The transitions at 730.4(3) and 890.7(3) keV were already observed by Daugas *et al*. [28] in the decay of an 8^+ isomer in ^{78}Zn, produced via fragmentation of a ^{86}Kr beam on a ^{nat}Ni target. Their deduced decay scheme is a cascade of four γ rays, of which the two lowest transitions are the 729.6(5) and 889.9(5) keV γ rays. The other two γ rays of 908.3(5) and 144.7(5) keV are not observed in our spectra (Fig. 7). Furthermore, the only other information about excited states in ^{78}Zn comes from a β-decay study of ^{78}Cu by Lund *et al*. [27]. However, none of the reported γ rays are present in our spectra (216, 524, and 737 keV).

TABLE VI. Energy values, peak areas from the on- (A_{on}) and off-resonance (A_{off}) β-gated spectra, relative intensities (I_{rel}), and half-live values of the resonant lines at mass 78.

Label	E (keV)	A_{on}	A_{off}	I_{rel}	$T_{1/2}$ (s)
1	114.9(2)	900(143)	–	100(16)	0.26(12)
2	730.4(3)	169(102)	–	54(33)	0.11(11)
3	890.7(3)	346(81)	158(72)	56(44)	0.37(21)

The coincidence relations of the resonant γ rays are treated in the same way as described in previous sections, using background-subtracted γ-ray spectra gated on the different γ rays under a prompt TAC condition. This time, an extra Time to Digital Convertor (TDC) condition was set, limiting the list-mode data only to events from the first 1000 ms of the implantation-decay cycle thereby reducing the long-lived activities. The results are summarized in Table VII. The 114.9 keV line shows a clear coincidence with a 688.7(3) keV transition. No coincidence with the 730.4 nor 890.7 keV transitions is observed. Part of the γ-ray spectra gated on the 730.4 and 890.7 keV transitions are shown in Fig. 8. One can clearly observe that these lines are mutually coincident and thus are in cascade. No other coincident γ rays were found in these spectra. In particular, note the absence of a 908.3 keV

TABLE VII. Coincident transitions of the resonant γ rays. Peak areas are shown in parentheses.

E (keV)	Coincident γ rays
114.9(2)	689(35)
730.4(3)	891(26)
890.7(3)	730(22)

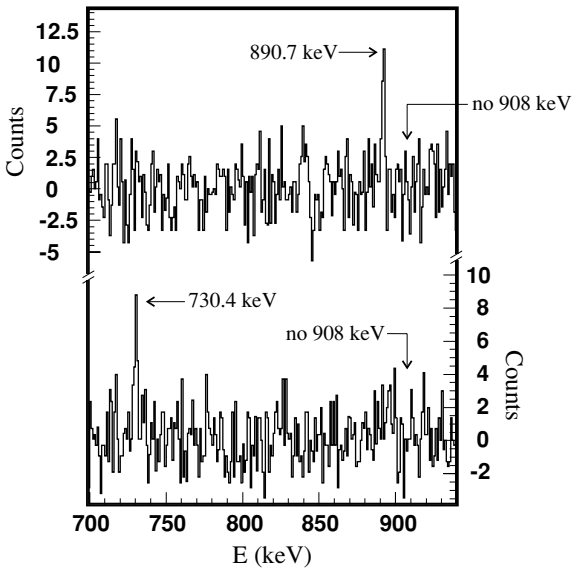

FIG. 8. Background corrected γ-ray spectra gated on the 730.4 (top) and 890.7 keV (bottom) γ rays.

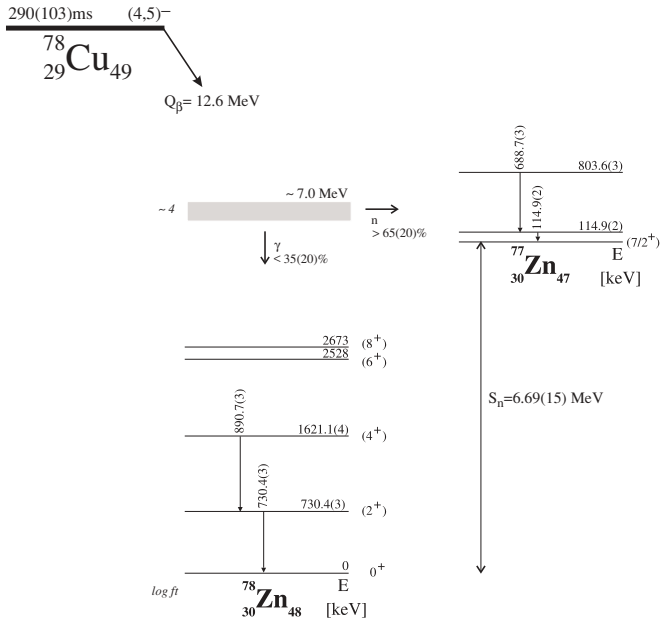

FIG. 9. Deduced decay scheme of ^{78}Cu, populating excited states in ^{78}Zn and, after neutron emission, excited states in ^{77}Zn. The (6^+) and (8^+) levels were observed by [28] but not in this work. The Q value and neutron separation energy were taken from [30].

γ ray, which was observed in cascade to the 730.4 and 890.7 keV lines by Daugas *et al*. [28]. From the γ-ray gated spectra, we can estimate an upper limit for the relative intensity (relative to Table VI) of the 908.3 keV γ ray, yielding $I_{\rm rel} < 20(7)\%$.

From the coincidence relations, it follows that the 114.9 keV is not related to the 730.4–890.7 keV cascade, and it is therefore more likely that this γ ray is populated via β-delayed neutron emission to ^{77}Zn. Indeed, a 114.6(3) keV γ ray was observed in the mass $A = 77$ data, and it was attributed to the decay of ^{77}Cu [10], based on the observed half-life in that work. A weak line at 687(1) keV was also observed in coincidence with the 114.6 keV γ ray, agreeing with the above coincidence relations. Hence, the 114.9 and 688.7 keV transitions are populated after β-delayed neutron emission of ^{78}Cu.

Since the intensities of the 730.4 and 890.7 keV transitions are equal, the order of the two γ rays is unclear. The same problem arose in [28], where the 729.6 keV transition was suggested to be the lowest transition, based on systematics. From a recent Coulomb excitation measurement using a post-accelerated ^{78}Zn beam from ISOLDE, it was shown that the 730.4 keV line is indeed the ground-state transition [29]. The final results are summarized in Fig. 9.

The Q_β value and neutron separation energy S_n, shown in Fig. 9, are taken from [30]. The intense β-delayed neutron branch, observed via the 114.9 keV γ ray (see below), indicates that one or several ^{78}Zn levels at high energy ($\gtrsim$7 MeV) get a large fraction of the β branching. Typically, transitions with a large β branching have a log $ft \sim 4$. It was calculated for ^{78}Cu that the energy of a level having a log ft of 4 and a β-branching ratio of 100% is $\sim$6 MeV. This value is indeed close to the neutron separation energy. Possibly, the β branching goes in reality to *several* high-energy states ($\gtrsim$7 MeV) in ^{78}Zn. Therefore, a grey zone at high energy are indicated in the decay scheme from Fig. 9.

From the intensity balance of the 114.9 keV γ ray and the ^{78}Zn γ rays, one can obtain a lower limit for the probability for neutron emission in ^{78}Cu: $P_n \geqslant 65(20)\%$.

Spin assignments shown in Fig. 9 are taken from [28]. Since both γ rays have equal intensities, the (2^+) level at 730.4 keV will get a negligible amount of β feeding from the ^{78}Cu mother nucleus. Furthermore, the 908.3 keV γ ray, depopulating the (6^+) state, was not observed: in neither the total spectra nor the γ ray gated coincidence spectra. Thus, the (6^+) state gets no or weak β feeding. Hence, the ^{78}Cu mother spin is most probably 4 or 5 since spins lower than 4 would give an enhanced $2^+ \rightarrow 0^+$ transition and spins higher than 5 would populate the complete $6^+ \rightarrow 4^+ \rightarrow 2^+ \rightarrow 0^+$ γ-ray cascade.

III. DISCUSSION

A. Systematics of the even-mass $^{70-78}$Cu isotopes

A discussion on the half-lives obtained from the β-delayed γ decay will not be carried out in this paper but will be part of a forthcoming paper, which will include the half-life results from this work and those from β-delayed neutron measurements on the even- and odd-mass Cu isotopes [17]. In this section, a detailed shell-model study on the variation of the energy levels in the odd-odd Cu isotopes considering different residual interactions is reported, and the results for the odd-odd Cu isotopes are compared with the suggested spin values established from the β-decay study. Note that β-decaying isomeric states other than the ground state were observed only in ^{70}Cu.

TABLE VIII. Energies of the proton single-particle states in ^{69}Cu, regarded as a ^{68}Ni core coupled with one valence proton [2].

π single-particle state	ϵ_{j_π} (MeV)
$1g_{9/2}$	2.553
$1f_{5/2}$	1.214
$2p_{1/2}$	1.110
$2p_{3/2}$	0.000

1. Residual interactions and shell-model study of the energy levels in the odd-odd Cu nuclei

In principle, the odd-odd nuclei ^{70}Cu–^{78}Cu can be described within the context of large-scale shell-model calculations. However, the need to consider the full *fp* shell and to include the $1g_{9/2}$ level leads to intractable model spaces. Since we concentrate on this particular set of five Cu nuclei, in which the filling of the neutron $1g_{9/2}$ orbital is playing an essential role, we consider these nuclei as consisting of an inert $^{68}_{28}$Ni$_{40}$ core coupled with the respective valence nucleons. This implies that there is only one valence proton and up to nine valence neutrons. The model space for the proton consists of the *pf* orbitals $2p_{3/2}$, $1f_{5/2}$, and $2p_{1/2}$, and $1g_{9/2}$; the neutrons will fill the $1g_{9/2}$ orbital. The energies ϵ_{j_π} of the proton single-particle states mentioned above are determined from the experimental data in ^{69}Cu as discussed in [2,13]. They are given in Table VIII.

The energy levels in the schematic approach are obtained in the following way. The proton single-particle energies have to be corrected for the monopole shift [5]: when the neutrons start filling the $1g_{9/2}$ single-particle level, the relative proton single-particle energies change because of the larger radial overlap between the proton $1f_{5/2}$ and neutron $1g_{9/2}$ orbitals compared to the overlap between the proton $2p_{3/2}$, $2p_{1/2}$ orbitals and the neutron $1g_{9/2}$ orbital. These corrected single-proton energies $\tilde{\epsilon}_{j_\pi}$ are expressed as

$$\tilde{\epsilon}_{j_\pi} = \epsilon_{j_\pi} + 10 n_{1g_{9/2}} E_{j_\pi, 1g_{9/2}}, \tag{1}$$

with

$$E_{j_\pi, 1g_{9/2}} = \frac{\sum_J \langle j_\pi, 1g_{9/2}; J|V|j_\pi, 1g_{9/2}; J\rangle (2J+1)}{\sum_J (2J+1)}, \tag{2}$$

which describes the average matrix element of the proton-neutron interaction (pure particle-particle matrix element), and

$$n_{1g_{9/2}} = \frac{N-40}{10} \tag{3}$$

is the occupation probability of the $\nu 1g_{9/2}$ single-particle level. This change in single-proton energy is illustrated in Fig. 10. The $1f_{5/2}$ orbital comes down in energy relative to the $2p_{1/2}$ and $2p_{3/2}$ orbitals. If one uses a residual quadrupole-quadrupole force, monopole shifts become trivially zero. To improve the realistic character of the schematic study using the residual quadrupole-quadrupole interaction, the monopole energy shifts obtained with the zero-range δ interaction are used.

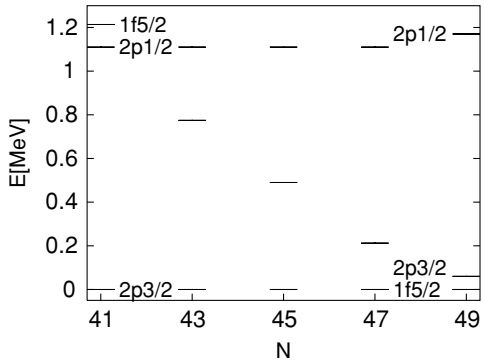

FIG. 10. Dependence on the neutron number N of the proton single-particle energies in the Cu isotopes, taking into account the monopole shift [5].

The filling of the neutron $1g_{9/2}$ orbital can, to a good approximation, be described by means of a one-quasiparticle excitation with energy $E_{1g_{9/2}}$ [31].

Besides the neutron one-quasiparticle energy and proton single-particle energies, we also need the two-body matrix elements coupling the proton j_π with the filling neutron $1g_{9/2}$ orbital to compute the energy levels. The filling of the neutron $1g_{9/2}$ orbital is approximated by a neutron one-quasiparticle configuration (indicated by the tilde, hence, $\widetilde{1g_{9/2}}$). These matrix elements can be expressed as

$$\begin{aligned}\langle j_\pi, \widetilde{1g_{9/2}}; J|V|j_\pi, \widetilde{1g_{9/2}}; J\rangle = {} & n_{1g_{9/2}} \langle j_\pi, 1g_{9/2}; J| \\ & \times V|j_\pi, 1g_{9/2}; J\rangle \\ & + (1 - n_{1g_{9/2}}) \langle j_\pi, 1g_{9/2}^{-1}; J| \\ & \times V|j_\pi, 1g_{9/2}^{-1}; J\rangle. \end{aligned} \tag{4}$$

This is a linear combination of particle-particle and particle-hole matrix elements, and as such, particularly sensitive to the filling of the neutron orbital. So the interaction changes from a pure particle-particle interaction in $^{70}_{29}$Cu$_{41}$ to a pure particle-hole interaction in $^{78}_{29}$Cu$_{49}$.

The energy of a particular configuration with a proton moving in the orbital j_π and the neutrons filling the $1g_{9/2}$ orbital is then expressed as

$$E_{1g_{9/2}} + \tilde{\epsilon}_{j_\pi} + \langle j_\pi, \widetilde{1g_{9/2}}; J|V_{\delta/QQ}|j_\pi, \widetilde{1g_{9/2}}; J\rangle. \tag{5}$$

In the present study, we focus on the proton $\pi 2p_{3/2}$ and $\pi 1f_{5/2}$ orbitals coupled to the neutron orbital $\nu 1g_{9/2}$. This gives rise to a multiplet with spin and parity of 3^-, 4^-, 5^-, 6^-, and 2^-, 3^-, 4^-, 5^-, 6^-, 7^-, respectively. Including also the nondiagonal matrix elements and diagonalizing the small matrices, we can obtain the final energy spectrum. We investigate the evolution of the energy levels as a function of neutron number and discuss the results in the next subsection. In this highly truncated model space, we study the effect of two different schematic interactions between the valence proton and the valence neutrons.

At first, we consider the effect of a quadrupole-quadrupole (QQ) proton-neutron interaction, defined as

$$V_{\mathrm{QQ}} = \chi \left(\sqrt{\frac{m\omega}{\hbar}} r_\pi\right)^2 \left(\sqrt{\frac{m\omega}{\hbar}} r_\nu\right)^2 \vec{Y}_2(\Omega_\pi) \cdot \vec{Y}_2(\Omega_\nu), \tag{6}$$

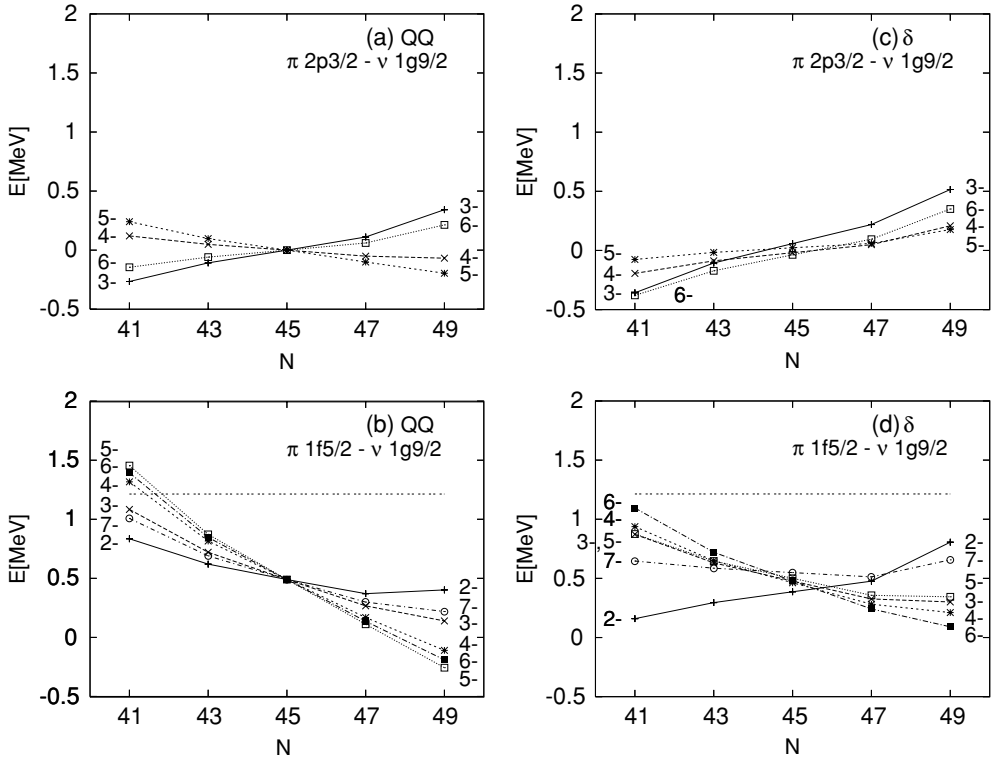

FIG. 11. Independent $\pi 2p_{3/2}\nu\widetilde{1g}_{9/2}$ and $\pi 1f_{5/2}\nu\widetilde{1g}_{9/2}$ multiplets in the Cu isotopes, using a quadrupole interaction [(a) and (b), respectively] and a δ interaction [(c) and (d), respectively]. The horizontal dashed line indicates the 1.214 MeV $\pi 1f_{5/2}$ level of ^{69}Cu.

where the strength $\chi = -0.02$ MeV. The strength has been obtained by fitting the theoretical $\pi 2p_{3/2}\nu 1g_{9/2}$ multiplet splitting to the experimental splitting in the lowest-lying levels in ^{70}Cu. This strength then fixes the structure of other proton-neutron multiplets and also their relative variation as a function of neutron number.

Secondly, we study the effect of a zero-range δ interaction with spin exchange, where the interaction has the form

$$V_\delta = -V_{\text{eff}}(1 - \alpha + \alpha\vec{\sigma}_\pi \cdot \vec{\sigma}_\nu)\delta(\vec{r}_\pi - \vec{r}_\nu), \tag{7}$$

with V_{eff} the strength of the interaction, equal to $V_{\text{eff}} = 400$ MeV fm^3. The amount of spin exchange is determined by the parameter α, which can vary from 0 to 1, and equals $\alpha = 0.1$ in the present calculations.

Finally, a large-scale shell-model calculation was performed using the realistic force determined by Hjorth-Jensen, Kuo, and Osnes [11], with the ANTOINE code [12,32]. Naturally, we no longer use a highly restricted model space but a larger one: the full p shell and the $1f_{5/2}$, $1g_{9/2}$ orbitals, for both protons and neutrons. The input values for the neutron and proton single-particle energies differ from the ones we used in the schematic study: now we use the single-particle energies of one neutron or one proton coupled to a $^{56}_{28}$Ni$_{28}$ core.

2. Discussion and comparison with the energy spectra of odd-odd Cu nuclei

In Fig. 11, we consider the multiplets $\pi 2p_{3/2}\nu\widetilde{1g}_{9/2}$ (a) and $\pi 1f_{5/2}\nu\widetilde{1g}_{9/2}$ (b) in an independent way (no mixing) for the QQ interaction. A clear dependence on the neutron number N, hence the occupation probability $n_{1g_{9/2}}$, results, which is of course very much like the behavior encountered when applying Paar's parabolic rule [33]. One notices the switching of the multiplet ordering in each multiplet with respect to the $N = 45$ midshell situation from a particle-particle into a particle-hole energy spectrum. For the lowest levels, originating from the $\pi 2p_{3/2}\nu\widetilde{1g}_{9/2}$ multiplet, this implies a change of the 3^- and 6^- levels into the 5^- and 4^- levels as lowest-lying levels, which seems consistent with the experimental changes in possible ground-state spins. In constructing the energy splitting in the second multiplet $\pi 1f_{5/2}\nu\widetilde{1g}_{9/2}$, the relative energy spacing between the $1f_{5/2}$ and $2p_{3/2}$ orbitals as well as the monopole variation in this $1f_{5/2}$ level, compared to the reference value of 1.214 MeV (the dashed line in Fig. 11) used for the calculation in ^{70}Cu, has been included for the various neutron numbers.

We compare the above results for the QQ interaction with the results for the δ interaction shown in Figs. 11(c) and 11(d). The results are rather similar, but the symmetry with respect to the $N = 45$ midshell point no longer holds (because the particle-particle and particle-hole matrix elements are no longer related by a simple change in sign). Moreover, the ordering in the lowest multiplet $\pi 2p_{3/2}\nu\widetilde{1g}_{9/2}$ now gives the correct result when compared with the experimental energy spectrum observed in ^{70}Cu. This is probably due to the more realistic properties of the zero-range character of the δ interaction when comparing, e.g., the two-body matrix elements with those of the realistic interaction of [11].

In a next step, we go beyond lowest order and consider the coupling between the multiplets $\pi 2p_{3/2}\nu\widetilde{1g}_{9/2}$, $\pi 1f_{5/2}\nu\widetilde{1g}_{9/2}$,

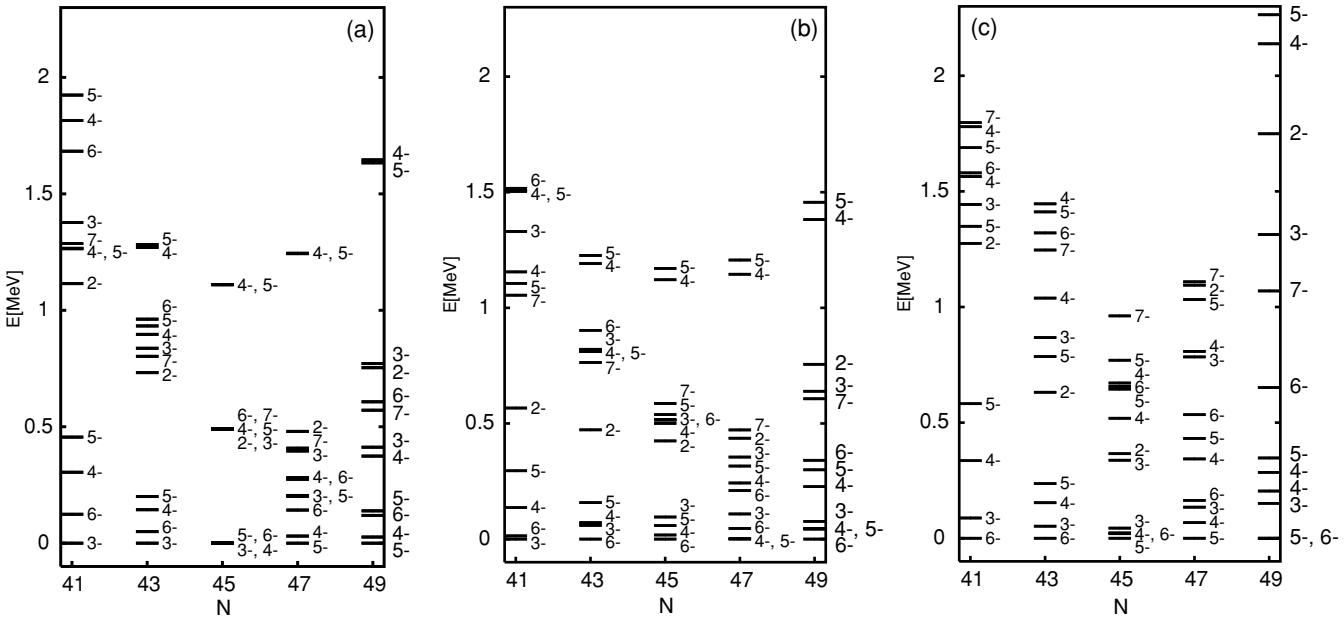

FIG. 12. Mixing of the $\pi 2p_{3/2}\nu\widetilde{1g}_{9/2}$, $\pi 1f_{5/2}\nu\widetilde{1g}_{9/2}$ and $\pi 2p_{1/2}\nu\widetilde{1g}_{9/2}$ multiplets in the Cu isotopes, using a QQ interaction (a) and a δ interaction (b), compared to the results obtained from the large-scale diagonalizations using a realistic interaction [11] (c).

and $\pi 2p_{1/2}\nu\widetilde{1g}_{9/2}$ explicitly. The results, derived by diagonalizing the small energy matrices, are presented in Fig. 12, for both a quadrupole-quadrupole (a) and a zero-range δ (b) interaction. The results become slightly more realistic but no major changes show up in the spectrum, compared to the results derived from the independent multiplets only. The general outcome remains the turning over of the multiplet ordering going from a specific particle-particle character (at $N = 41$) toward the reversed ordering corresponding with the particle-hole character (at $N = 49$).

A comparison is also made with the results obtained using the realistic interaction determined by [11] (using the shell-model code ANTOINE [12,32]). The resulting energy spectrum is displayed in Fig. 12(c).

One notices that the relative ordering of the 3^- and 6^- levels is reversed compared to the experimental situation in ^{70}Cu for both schematic interactions. For the δ interaction, the energy difference becomes tiny, whereas the realistic force correctly describes the experimental ordering. For the position of the experimental 2^- state (again in ^{70}Cu), the specific J dependence in the two-body matrix elements using a δ interaction seems to account much better for this result, compared to the QQ interaction. Here, the realistic force predicts the 2^- level too high in excitation energy. This clear deviation seems to be related to a much stronger configuration mixing present in the wave function for the lowest 2^- and 7^- states [the $(\pi_{1f5/2}\nu_{1g9/2})$ component is not the dominant one] and to the specific character of the interaction derived in [11].

From the three calculations, it is clear that the first 5^- state comes down in excitation energy as the neutron number increases and even becomes the ground state in ^{78}Cu (in close agreement with the indications from the present experiments). The second 4^- state has also come down very much, as has the second 5^- state. It is rather remarkable that the lowest energy states in ^{78}Cu are the ones with relatively high spin, but this comes from the change of particle-particle to particle-hole behavior.

When we compare the level structure in Fig. 12 with the levels suggested by the experiment, we remark that in general the theoretical results predict low-lying levels with higher spins than the experiment would suggest.

There is at present very little information about the ground-state spin and parity value for the isotopes lying in between, i.e., ^{72}Cu, ^{74}Cu, and ^{76}Cu: the theoretical calculations suggest ground states that (in the light of the accuracies in the above theoretical descriptions) might be consistent with an overall value of 3^-. This would not be inconsistent with the present assignments of (1–3) in ^{72}Cu [34], (2,3) in ^{74}Cu, and (3,4) in ^{76}Cu, but more detailed experimental studies of these odd-odd Cu nuclei are needed in order to learn about the characteristics of the proton-neutron interaction as well as the monopole shifts in this particular region of the nuclear chart.

B. Systematics of the even-mass $^{70-78}$Zn Isotopes

In Fig. 13, a compilation of all known $^{\text{even}}$Zn levels is shown. Data were taken primarily from the Evaluated Nuclear Structure Data File (ENSDF) database (see [35]). New levels given in two recent papers [36] and [28] for ^{70,72}Zn and ^{78}Zn, respectively, are not yet included in the ENSDF database, but they are drawn in the figure as well. In addition, for mass numbers $70 \leqslant A \leqslant 78$, the information from this work was also included. Since several levels from the literature were found to be in conflict with our observations, as described above, these levels are not drawn in Fig. 13. Furthermore, we omitted the levels at 1068.3(2) keV in ^{70}Zn and 670(30) and 1840(50) keV in ^{74}Zn from literature because they are most likely the 1070.73(9), 606.01(5), and 1789(1) keV levels

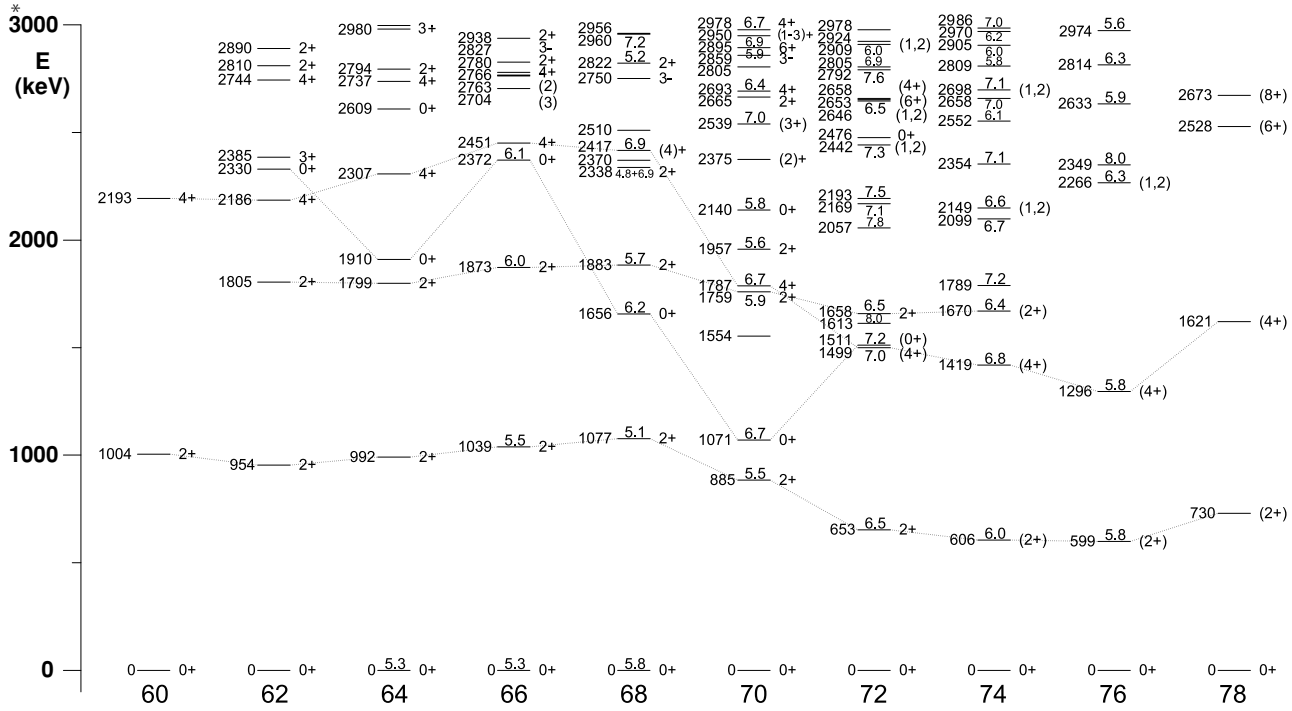

FIG. 13. Compilation of excited states in ^{even}Zn nuclei, as a function of the mass number A (see text). States are labeled with the energy (left), spin-parity (right), and log ft value (middle) when available. The data are mostly from [2,28,34–36]. The levels at 1789, 2149, 2354, 2658, 2698, and 2986 keV in ^{74}Zn and at 2266 and 2349 keV in ^{76}Zn are from this work.

from our work given the high uncertainties in their energy. The quoted uncertainty for the 1068.3(2) keV level does not allow us to associate this level with the 1070.73(9) keV level. According to the Nuclear Data Sheets [37], this level was observed in several reaction experiments: (t,p), $(n,n'\gamma)$, $(d,{}^3\mathrm{He})$, (p,p'), and $(p,p'\gamma)$. It is, however, not clear where its precision comes from. In most cases, the observation of the level is based on charged-particle detection instead of γ-ray detection with a germanium detector which, in general, has a worse energy resolution. The energy determination in our work is based on the 185.85(3) keV γ-ray transition, feeding into the 884.88(9) keV level; but an energy calibration mismatch at low energy cannot be ruled out. Yet, we note that in [38] a 185.9 keV γ ray was detected, determining the level at 1070.8 keV, which is in good agreement with our value. Therefore, we ignore the earlier energy assignment and consider the 1068.3 keV level as being the same as the 1070.73(9) keV level.

As a guide for the next discussion, we present in Table IX the ratios of the energies of the 0_2^+, 2_2^+, and 4_1^+ states to the energy of the 2_1^+ state. In case of a pure harmonic vibrator this value should be two. The ratio is slightly higher than two for the 4_1^+ states, but stays rather constant over a wide range of neutron numbers ($N = 30$ to $N = 48$). In the case of the 2_2^+ state, the situation is different. For the Zn isotopes with $N \leqslant 40$, the ratio is slightly lower than two but again rather constant. This might hint to a certain degree of anharmonicity present in the Zn isotopes. However, the situation changes dramatically when neutrons are added beyond $N = 40$. The ratio for the 2_2^+ states rises toward 3, indicating a rather abrupt change in their structure. The energy of the 0_2^+ state reaches a minimum at $N = 40$. This situation is very similar to the neighboring nickel ($Z = 28$) isotopes where the 0_2^+ state becomes the first excited state in $^{68}_{28}\mathrm{Ni}_{40}$ [23]. Also, the $N = 48$ and $N = 50$ isotones show a similar behavior around $Z = 40$.

TABLE IX. Energy ratios of the 0_2^+, 2_2^+, and 4_1^+ excited states with respect to the 2_1^+ state for all known even-mass zinc isotopes.

I^π	^{A}Zn	60	62	64	66	68	70	72	74	76	78
	$N =$	30	32	34	36	38	40	42	44	46	48
0_2^+		–	2.4	1.9	2.3	1.5	1.2	2.3	–	–	–
2_2^+		–	1.9	1.8	1.8	1.7	2.0	2.5	2.8	–	–
4_1^+		2.2	2.3	2.3	2.4	2.2	2.0	2.3	2.3	2.2	2.2

The occurrence of the minimum at N or $Z = 40$ is obviously related to the presence of the subshell, but it is not yet fully understood what actually causes it. Arguments in literature can be found, e.g., that a neutron pair excitation from the pf shell to the $1g_{9/2}$ orbital is lowered in energy because of the strong coupling of the pair in this $1g_{9/2}$ orbital and because of the large phase space available [39]. In a recent paper, the ^{68}Ni was claimed to have a superfluid neutron shell [40] that may cause the 0_2^+ state to be a mixture of different 0^+ configurations, formed by pairs of nucleons located in different orbitals. Possibly, this effect causes the 0_2^+ state in ^{68}Ni to be lowered in energy. Similar effects might indeed be present in the zinc isotopes and $N = 48$ and $N = 50$ isotones.

Finally, it should be noted that the energy of the 2_1^+, 2_2^+, and 4_1^+ states lowers in energy for $N \geqslant 40$. Possibly, it is related

to a change in pairing energy, i.e., the energy needed to break up a coupled pair of nucleons; to a change in strength of the short-range component of the nucleon-nucleon interaction; or to the presence of collective effects, which are maximum at mid-shell ($N = 45$) and minimal near the semi-magic $N = 40$ and magic $N = 50$ neutron number. The latter was suggested to explain the trend observed in the experimental $B(E2)$ values in ^{70,72}Zn [6]. The recent Coulomb excitation experiments that have extended these measurements toward ^{74,76,78}Zn [29] using the post-accelerated beams from ISOLDE will certainly shed more light on this problem.

Because of the nature of ^{78}Zn two-proton particles and two neutron holes away from the doubly magic ^{78}Ni nucleus, some comments can be made on its β decay. The allowed β decay of ^{78}Cu to the ^{78}Zn daughter nucleus is expected to stem primarily from the conversion of a $\nu 1g_{9/2}$ neutron into a $\pi 1g_{9/2}$ proton. The ^{78}Zn daughter nucleus arrives in the $\pi 1f_{5/2}^{+1} 1g_{9/2}^{+1} \nu 1g_{9/2}^{-2}$ configuration, which forms a $(2\text{–}7)^-$ multiplet of states that is high in energy. Note that the β feeding was indeed found to populate mainly states at high-energy ($\geqslant$7 MeV). Possibly, it is the high Q_β value of ^{78}Cu (12.6 MeV) that allows strong β feeding to these states at high energy. Because of the spin selection rules of allowed β decay, only the states with spin 3–6 of the multiplet are selected by the—supposed $I^\pi = 4{,}5^-$—^{78}Cu mother. The states of this multiplet will further γ decay and arrive eventually in the $\pi 1f_{5/2}^{+2} \nu 1g_{9/2}^{-2}$ ground-state configuration of ^{78}Zn, passing by the 2^+ and 4^+ states at 730 and 1621 keV, respectively. The latter two states presumably consist partly of this ground-state configuration.

IV. CONCLUSION

A β-decay study of the ^{74,76,78}Cu isotopes produced in high-energy proton-induced fission of ^{238}U, ionized with resonant laser ionization, and mass separated is reported. The level systematics of the even-even Zn isotopes was extended and is discussed all the way down to ^{78}Zn, two protons and two neutrons away from the doubly magic ^{78}Ni nucleus. From the energies of the first 2^+, 0^+, and 4^+ states, it is apparant that the Zn nuclei change character rather abruptly at $N = 40$. The origin of this change is not fully understood and cannot be determined from the energy level systematics only. Transition matrix elements [$B(E2\text{: } 2^+\text{–}0^+)$] from Coulomb excitation measurements using energetic Zn beam isotopes will shed light on this problem [29]. Half-life values and limits on spin values for the odd-odd Cu isotopes were obtained from the characteristic feeding patterns in the β decay. Important to note is that in contrast to ^{70}Cu, where three β-decaying isomers were reported, no isomers were observed in the other Cu isotopes in spite of the same production and ionization mechanism used. A detailed shell-model study of the levels of the odd-odd Cu isotopes from $N = 41$–49 was performed using different residual interactions. Schematic δ and QQ interactions in a highly restricted model space as well as realistic forces using the full p shell and $1f_{5/2}$, $1g_{9/2}$ orbitals for protons and neutrons were used. The obtained results are consistent with the suggested spins of the odd-odd Cu isotopes. More detailed experimental information on the ground-state properties of the Cu isotopes obtainable via in-source laser ionization [9] is needed.

ACKNOWLEDGMENTS

We gratefully acknowledge the ISOLDE technical group for assistance during the experiment. This work was supported by the Inter-University Attraction Poles (IUAP), Belgium, under Project No. P5/07 and the FWO-Vlaanderen, Belgium. K.V.d.V. is Research Assistant of the FWO-Vlaanderen. U.K. was supported by the "Beschleunigerlabor der TU and LMU München" and the EU (Contract ERBFMGEECT 980120).

[1] J. Van Roosbroeck *et al*., Phys. Rev. Lett. **92**, 112501 (2004).
[2] J. Van Roosbroeck *et al*., Phys. Rev. C **69**, 034313 (2004).
[3] K.-H. Langanke *et al*., Phys. Rev. C **67**, 044314 (2003).
[4] H. Grawe and M. Lewitowicz, Nucl. Phys. **A693**, 116 (2001).
[5] N.-A. Smirnova *et al*., Phys. Rev. C **69**, 044306 (2004).
[6] S. Leenhardt *et al*., Eur. Phys. J. A **14**, 1 (2002).
[7] M. Hannawald *et al*., Phys. Rev. Lett. **82**, 1391 (1999).
[8] K.-H. Langanke *et al*., Phys. Rev. Lett. **90**, 241102 (2003).
[9] L. Weissman *et al*., Phys. Rev. C **65**, 024315 (2002).
[10] J.-C. Thomas *et al*. (unpublished).
[11] M. Hjorth-Jensen, T.-T.-S. Kuo, and E. Osnes, Phys. Rep. **261**, 125 (1995).
[12] E. Caurier, computer code ANTOINE, IRES, Strasbourg, 1989–2002.
[13] J. Van Roosbroeck *et al*., in *Proceedings of the Third International Conference on Exotic Nuclei and Atomic Masses ENAM 2001*, edited by J. Äystö, P. Dendooven, A. Jokinen, and M. Leino (Springer Verlag, Berlin, 2002), p. 327.
[14] E. Kugler *et al*., Hyp. Int. **129**, 23 (2000).
[15] R. Catherall *et al*., Nucl. Instrum. Methods Phys. Res. B **204**, 235 (2003).
[16] V.-N. Fedoseyev *et al*., Hyp. Int. **127**, 409 (2000).
[17] D. Pauwels *et al*. (unpublished).
[18] U. Köster, Ph.D. thesis, TU München, 2000.
[19] J.-A. Winger *et al*., Phys. Rev. C **39**, 1976 (1989).
[20] K.-L. Kratz *et al*., Z. Phys. A **340**, 419 (1991).
[21] M. Bernas *et al*., Nucl. Phys. **A413**, 363 (1984).
[22] R. Haupt *et al*., Z. Phys. A **317**, 193 (1984).
[23] R. Firestone, *Table of Isotopes,* 8th ed. (Wiley, New York, 1996)
[24] A.-R. Farhan, Nucl. Data Sheets **74**, 529 (1995).
[25] J.-A. Winger *et al*., Phys. Rev. C **42**, 954 (1990).
[26] B. Singh *et al*., Nucl. Data Sheets **74**, 63 (1995).
[27] E. Lund *et al*., in Proceedings International Conference on Nuclei Far From Stability, Lake Rosseau, Ontario, Canada, 1987 (unpublished), p. 587.
[28] J.-M. Daugas *et al*., Phys. Lett. **B476**, 213 (2000).
[29] P. Mayet *et al*. (unpublished).
[30] G. Audi, A.-H. Wapstra, and C. Thibault, Nucl. Phys. **A729**, 337 (2003).
[31] P. Ring and P. Schuck, *The Nuclear Many-Body Problem* (Springer, New York, 1980).

[32] E. Caurier and F. Nowacki, Acta Phys. Pol. B **30**, 705 (1999).
[33] V. Paar, Nucl. Phys. **A331**, 16 (1979).
[34] J. Thomas *et al*. (unpublished).
[35] National Nuclear Data Center, Brookhaven National Laboratory, http://www.nndc.bnl.gov/nndc/nudat/.
[36] A.-N. Wilson *et al*., Eur. Phys. J. A **9**, 183 (2000).
[37] M.-R. Bhat, Nucl. Data Sheets **68**, 124 (1993).
[38] S. Franchoo, Ph.D. thesis, K.U. Leuven, 1999.
[39] M. Bernas *et al*., Phys. Lett. **B113**, 279 (1982).
[40] O. Sorlin *et al*., Phys. Rev. Lett. **88**, 092501 (2002).